RESEARCH ARTICLE

ADVANCED
ELECTRONIC
MATERIALS
Open Access

Check for updates

www.advelectronicmat.de

A Multilevel Magnetic Synapse Based on Voltage-Tuneable Magnetism by Nitrogen Ion Migration

P. Monalisha,* Zheng Ma, Eva Pellicer, Enric Menéndez, and Jordi Sort*

Advanced synaptic devices with simultaneous memory and processor capabilities are envisaged as core elements of neuromorphic computing (NC) for low-power artificial intelligence. So far, most synaptic devices are based on resistive memories, where the device resistance is tuned with applied voltage or current. However, the use of electric current in such resistive devices causes significant power dissipation due to Joule heating. Higher energy efficiency has been reported in materials exhibiting voltage control of magnetism (VCM). In particular, voltage-driven ion motion to modulate magnetism (magneto-ionics) is an emerging VCM mechanism that can offer new prospects for low-power implementation of NC. In the present work, voltage-driven nitrogen ion motion is exploited in transition metal nitride (CoFeN) thin films (i.e., nitrogen magneto-ionics) to emulate biological synapses. In the proposed device, distinct multilevel non-volatile magnetic states for analog computing and multi-state storage are realized. Moreover, essential synaptic functionalities of the human brain are successfully simulated. The device exhibits an excellent synapse with a remarkable retention time ($\approx$6 months), high switching ratio and large endurance ($\approx10^3$), for hardware implementation of NC. This research provides new insight into exploiting magneto-ionic-based synaptic devices for spin-based neuromorphic systems.

1. Introduction

In the present era of artificial intelligence (AI) and the Internet of Things (IoT), computers based on the conventional von Neumann architecture, where the memory and processing units are placed separately, face important bottlenecks in terms of attainable speed and energy efficiency.[1] As an alternative, in an attempt to cope with the current technological needs, a new computing paradigm emulating how the human brain works, with synchronized memory and processing units, is emerging. However, much progress is still needed to optimize the key components of brain-inspired neuromorphic computing (NC): the artificial synapses, which are central to learning and memory. Tremendous progress has been made to fabricate synaptic devices exploiting various mechanisms including ferroelectric memory (Fe-RAM),[2,3] phase change memory (PCM),[4,5] resistive random-access memory (ReRAM),[6,7] electrolyte-gated transistors (EGT),[8,9,10] etc.

Along with charge-based devices, synaptic devices exploiting their spin degree of freedom have been studied recently.[11,12,13,14] Devices based on spin-transfer-torque magnetic random memory (STT-MRAM),[15,16] skyrmion,[17–19] and spin-orbit-torque magnetic random memory (SOT-MRAM),[20,21,22] etc have been implemented in synaptic electronics. The spintronics materials are appealing for their fast switching, unlimited endurance and compatibility with the complementary metal oxide semiconductors (CMOS) based technology.[20,23] However, in these magnetic synapses, a large fraction of energy is dissipated in the form of heat due to the Joule effect arising from the electric currents needed to switch the memory units and poses important limitations in terms of energy efficiency.[24] In this context, a new type of magnetic synapse operating with voltage, with minimized flowing current, might significantly boost energy efficiency. In this regard, materials whose magnetic properties can be directly controlled with voltage (through the inverse magnetoelectric effect), could be a good alternative.[25]

Magneto-ionics, defined as voltage control of magnetism via ion (O^{2-},[26,27] Li^+,[28,29] H^+,[30,31]) migration, has acquired a leading role in magnetoelectric systems since it can cause massive modulation of the magnetic properties in a permanent way. However, one of the drawbacks of this mechanism is the limited switching speed attainable at room temperature, which is still rather slow (often > ms), because ion diffusion is a thermally-activated process.[32] Voltage-driven H^+ ion transport has been reported to be faster (in some cases < 100 µs),[33] but H^+ magneto-ionic effects can be highly sensitive to

P. Monalisha, Z. Ma, E. Pellicer, E. Menéndez, J. Sort
Departament de Física
Universitat Autònoma de Barcelona
Cerdanyola del Vallès, Barcelona E-08193, Spain
E-mail: monalisha.peda@uab.cat; jordi.sort@uab.cat
J. Sort
Institució Catalana de Recerca i Estudis Avançats (ICREA)
Pg. Lluís Companys 23, Barcelona E-08010, Spain

environmental humidity leading to limited retention times.[30] Recently, nitrogen magneto-ionics has proven to be also more efficient than O^{2-} magneto-ionics in terms of induced magnetization modulation, switching speed, and cyclability.[34] Nitrogen magneto-ionics has been observed in binary and ternary transition metal (TM) nitrides.[31,35] Remarkably, compared to the binary TM nitrides, the ternary TM nitrides often show a much larger magneto-ionic response due to synergetic microstructural/ion diffusion and electric resistivity effects.[35] Recently, magneto-ionic-based synaptic devices have been reported using CoN, and only frequency-dependent behavior has been shown. However, complete emulation of a wide range of synaptic functionalities is yet to be validated for the potential neuromorphic application of magnetic synapses. Additionally, a high dynamic range, faster switching, good endurance and excellent retention are the important figure of merits of a synaptic device for real-life technological applications. Besides, multilevel non-volatile states are crucial for analogue computing and high-density data storage. Due to its technological potential, a complete and systematic study on N^{3-} magneto-ionic-based synaptic devices is highly desirable.

In this work, we propose a two-terminal (2T) magneto-ionic synaptic device based on a ternary transition metal nitride thin film: $(Co_{35}Fe_{65})_xN_{1-x}$ (for simplicity, CoFeN). This material is capable of inducing a large magneto-ionic effect compared to its binary nitride counterparts. Moreover, $Co_{35}Fe_{65}$ is well known for its very high saturation magnetization and high magnetic anisotropy among all TM magnetic alloys at room temperature, thus promising for spin-based NC.[37,38] In the as-grown state, CoFeN is paramagnetic. However, the application of external voltage triggers the emergence of a net magnetic moment, which can be highly tuned through electrolyte gating (i.e., inducing a transition from paramagnetic to ferromagnetic states). A very high ON/OFF ferromagnetism switching ratio (with $M_S \approx 880$ emu cm^{-3}) and a high magneto-ionic speed (12.3 emu cm^{-3} s^{-1}) are achieved at room temperature. Based on this magneto-ionic performance, several neuromorphic functionalities have been demonstrated. First, we have realized multilevel non-volatile magnetized states for analog computing and multi-state storage, using a series of programmed pulses. Then, we successfully emulated various characteristic synaptic functions such as spike amplitude-dependent plasticity, spike duration-dependent plasticity, and long-term potentiation/depression. Interestingly, the device exhibits excellent figures of merit such as large endurance ($\approx 10^3$) and remarkable retention time (≈ 6 months) for practical NC application. Since reading can be done externally (i.e., using a magnetometer), this 2T device enables independent reading and writing operations, unlike other conventional 2T synaptic devices, that allow easy integration in crossbar arrays.[39] Finally, the working mechanism of the device has been probed using X-ray photoelectron spectroscopy (XPS). Our results highlight the excellent platform offered by magneto-ionics to mimic biological synapses for building artificial NC systems.

2. Results and Discussion

CoFeN thin films were deposited on Ti (20 nm)/Cu (60 nm) coated [100]-oriented Si substrate at room temperature using reactive magnetron sputtering (see Experimental Details). The CoFeN film thickness was fixed at 10 nm (i.e., relatively thin to enhance the magneto-ionic effect).[36] All the magneto-ionic measurements were carried out in a capacitor-like configuration at room temperature using a vibrating sample magnetometer (VSM). The schematics of the device structure and the electrical connections are presented in **Figure 1**a. The Cu/Ti buffer layer acted as the working electrode, while a Pt wire served as the counter electrode in the proposed device structure. An anhydrous propylene carbonate (PC) with dissolved Na$^+$ and OH$^-$ traces (10–25 ppm) was used as an electrolyte, which also acts as an N^{3-} ion reservoir. The working mechanism of the synaptic device is presented in Figure 1b. Upon voltage application, an electric double layer (EDL) is formed at the film/electrolyte interface, which induces a large electric field perpendicular to the film surface. The Na$^+$ ions dissolved in the liquid electrolyte facilitate the formation of a strong electric field due to their small ionic radius when the working electrode is negatively biased. The strong electric field drives N^{3-} ions into/out of the sample. The working mechanism involves both electrostatic effect and electrochemical reactions in the sample. With negative gating, the sample undergoes denitriding (removal of N^{3-} ions), assisted by the negative electric field. However, positive gating results in sample nitriding by re-insertion of N^{3-} ions from the liquid, assisted by a positive electric field. The nitriding and denitriding processes in CoFeN are reversible and can be accomplished multiple times by alternating voltages of opposite polarities.

To investigate the magnetic effects caused by N^{3-} ion motion, the CoFeN thin films were electrolyte-gated at room temperature and magnetic hysteresis loops were recorded in situ. All the magnetic measurements were carried out by applying the magnetic field parallel to the sample surface (in-plane). The magnetization (M) versus applied magnetic field (H) hysteresis measurements of the as-prepared and voltage-treated ($V_G = -12$ V) sample are presented in Figure 1c. The as-grown CoFeN films exhibit a virtually paramagnetic behavior, with a very small M_S (≈ 15 emu cm^{-3}) likely arising from the presence of residual metallic Fe or Co clusters, or from off-stoichiometric regions in the as-grown CoFeN films.[35] Upon voltage treatment (-12 V for 20 min), M_S increases dramatically, showing a clear paramagnetic-to-ferromagnetic switching. The M-H loop of the voltage-treated sample shows low coercivity (65 Oe) and large squareness ($M_R/M_S \approx 0.84$), suggesting in-plane anisotropy. The attained value of saturation magnetization by applying $V_G = -12$ V is $M_S \approx 880$ emu cm^{-3}. With negative voltage, M increases due to the extraction of N^{3-} ions from the sample, thereby reducing CoFeN (paramagnetic) to metallic CoFe (ferromagnetic).[34–36] Thus, CoFeN exhibits clear OFF→ON switching of ferromagnetism. Remarkably, the obtained ON/OFF ratio in CoFeN is considerably higher than previous values reported for binary FeN or CoN.[36]

The time evolution of M, while applying a gate voltage $V_G = -12$ V, is presented in Figure 1d. An in-plane magnetic field of 10 kOe was applied (well above the saturation magnetic field) throughout the measurement. M quickly increased during the first few seconds of voltage application and then saturates. The speed of magnetization was calculated to be 12.3 emu cm^{-3} s^{-1} by linearly fitting the initial part (first 10 s) of the M versus t curve, shown as an inset in Figure 1d. The high dynamic range

ADVANCED
SCIENCE NEWS
www.advancedsciencenews.com

ADVANCED
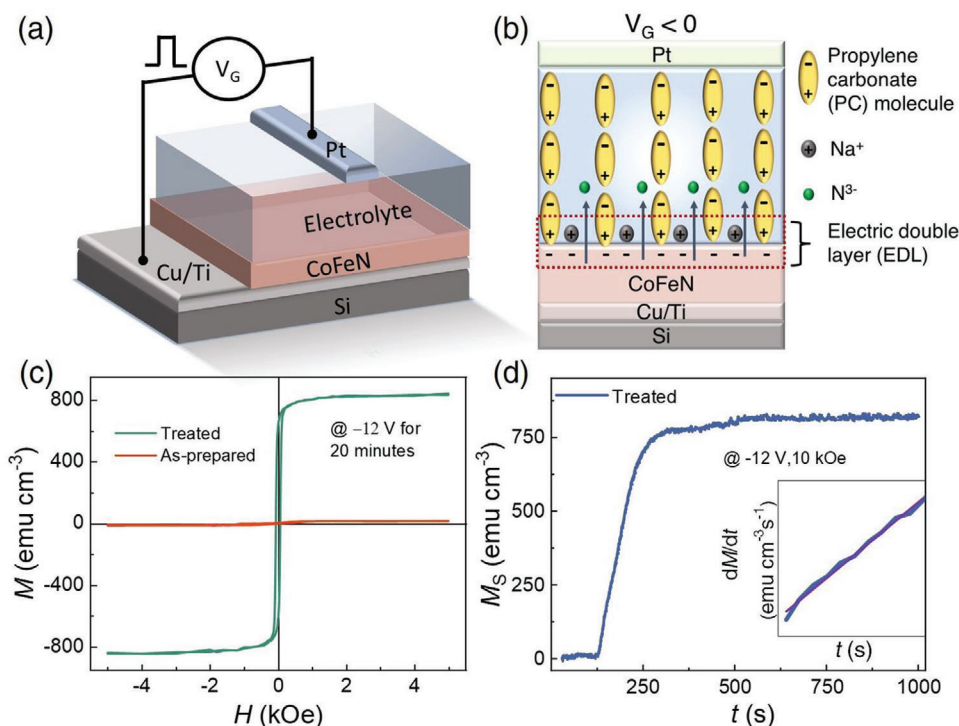ELECTRONIC
MATERIALS
www.advelectronicmat.de

Figure 1. a) Schematics of the CoFeN-based synaptic device and magneto-ionic measurement setup in a capacitor-like configuration. b) Schematics illustrating the working mechanism of the nitride system with negative voltage treatment involving both electrostatic and electrochemical effects. c) The M-H hysteresis loop of the CoFeN sample showing a paramagnetic to ferromagnetic switching with voltage treatment of -12 V for 20 min. d) The M-t curve of the sample with voltage (-12 V) treatment, and the inset show the linear fitting of the M-t curve to calculate the magneto-ionic speed.

(magnetization generation ratio ∼ 880 emu cm^{-3}) together with the high magneto-ionic speed ($\approx$12.3 emu cm^{-3} s^{-1}) makes CoFeN particularly promising for NC applications.

The mechanism underlying the magnetic switching in the investigated ternary nitride was probed using XPS, where the change in valence states of the elements was analyzed for samples before and after voltage treatment. The XPS spectra were recorded for the as-prepared and voltage-treated samples, after applying $V_G = -12$ V for 15 min. **Figure 2**a shows the Co 2p$_{3/2}$ core-level spectrum of the as-prepared CoFeN sample, evidencing the presence of only Co^{3+} (780.6 eV) peak.[40] On the contrary, the corresponding peak in the voltage-treated sample reveals the presence of metallic Co^0 (777.9 eV) along with the Co^{3+} peak in Figure 2b.[41] Similarly,
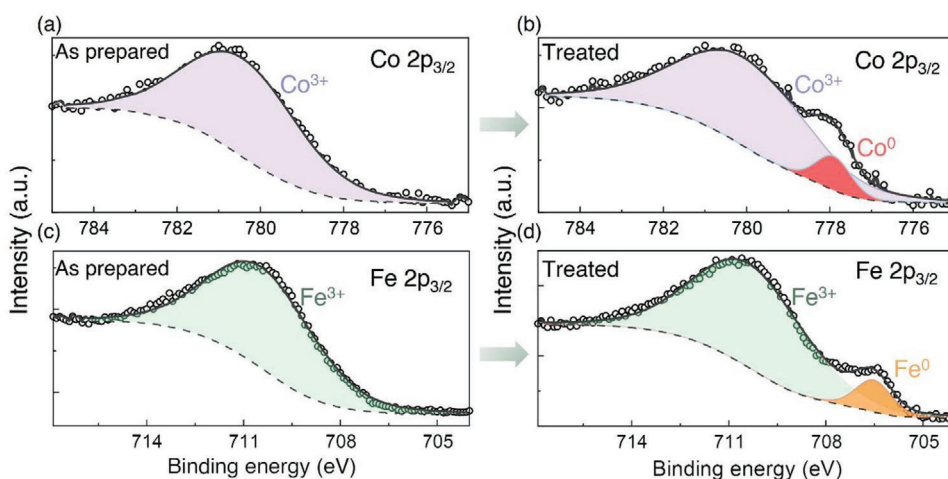

Figure 2. XPS spectra of the CoFeN surface. The sample was treated with $V_G = -12$ V for 15 min. a) Co 2p3/2 spectrum shows only the Co^{3+} peak in the as-prepared sample. b) Co 2p3/2 spectrum showing Co^{3+} and metallic Co^0 peaks in the voltage-treated sample. c) Fe 2p3/2 shows only the Fe^{3+} peak in the as-prepared sample. d) Fe 2p3/2 spectrum showing Fe^{3+} and metallic Fe0 peaks in the voltage-treated sample.
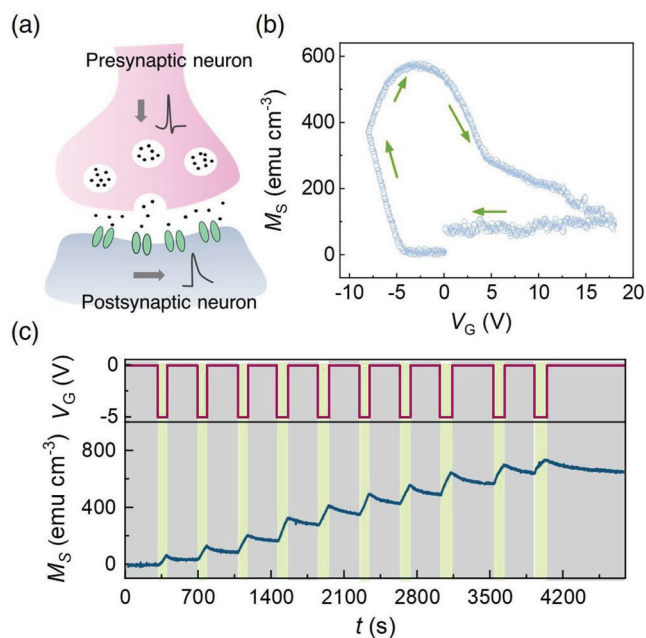
Figure 3. a) Schematics of a biological synapse demonstrating signal transmission from presynaptic to postsynaptic neurons. b) Variation of sample magnetization as a function of VG with a sweeping speed of 0.03 V s^{-1}, evidencing a non-volatile and reversible change. c) Multilevel non-volatile magnetic states were obtained by applying ten consecutive gate pulses (V_G = -5 V, t_P = 90 s) spaced apart by 300 s.

the Fe 2p$_{3/2}$ core-level spectrum of the as-prepared sample, presented in Figure 2c, illustrates the existence of only Fe^{3+} peak (710.6 eV).[42] Upon voltage treatment, there is the advent of metallic Fe^0 peak (706.5 eV) along with Fe^{3+} peak in the corresponding Fe 2p$_{3/2}$ spectrum (Figure 2d).[43] Thus, Figure 2(b,d) proves that, with negative voltage treatment, the sample undergoes denitriding, hence reducing CoFeN to ferromagnetic CoFe, in agreement with the magnetic results. Hence, the XPS study confirms the proposed working mechanism of the denitriding process.

In the human brain, the synapse is a functional connection between neurons that allows signal transmission. The schematics of biological synapses, allowing signal transmission from presynaptic neuron to postsynaptic neuron is depicted in **Figure 3**a. Synapses exhibit a fascinating property called "synaptic plasticity" (change of synaptic weight depending on activity level), which forms the basis for all learning and memory happening in the human brain.[44] In the present study, the magnetic switching (from paramagnetic to ferromagnetic) in the TM nitride-based device has been used to imitate various synaptic functionalities. Here, M switching is considered as the synaptic weight update and pulsed electric voltages as the external stimuli.

To demonstrate the neuromorphic properties of the investigated magneto-ionic material, we first measured the variation of M as a function of gate voltage by sweeping V_G in a clockwise fashion (from 0 to -8 V, then -8 to 0 V, then 0 to18 V, and finally back to 0 V), with a sweeping speed of 0.03 V s^{-1}, as shown in Figure 3b. An in-plane magnetic field of 10 kOe was applied throughout the measurement. The sample M increases with neg-

ative gating (sweeping from 0 to -8 V, and from -8 to 0 V,) due to the aforementioned sample denitriding by the removal of N^{3-} ions assisted by a negative electric field. Conversely, with positive gating, M decreases as the N^{3-} ions are inserted back into the sample, converting CoFe (ferromagnetic) back to CoFeN (paramagnetic). A small gap opening can be observed in Figure 3b, reflecting partial irreversibility. However, with a faster V_G sweeping fully closed loops can be obtained compromising the magnetization modulation, as shown in Figure S3 (Supporting Information). The M versus V_G curve results in a loop, representing the non-volatile and virtually reversible modulation of sample magnetization, making it suitable for the emulation of both short-term and long-term synaptic plasticity.

Multilevel non-volatile states are crucial for analog computing and to increase the memory density for neuromorphic computing applications.[45,46] Multilevel magnetic states have been made accessible in the CoFeN synaptic device by applying trains of negative pulses (V_G = -5 V, pulse duration t_P = 90 s), spaced apart by 300 s, as shown in Figure 3c. We can see that during the negative gating periods, M increases due to sample denitriding. However, in the periods when voltage is stopped, M slightly decreases but retains a progressively higher value after each step, evidencing an intrinsic non-volatile nature. Such spontaneous partial depletion of the generated M has been observed in other systems.[34] With successive pulses, CoFeN becomes progressively more denitrided, resulting in states with higher M_S. Hence, by applying programming voltage pulses, we could realize multiple discrete non-volatile states for NC applications.

Synaptic plasticity can be tuned by varying the amplitude of external stimuli. This is termed "spike amplitude-dependent plasticity" (SADP). SADP was mimicked in the CoFeN-based synaptic device by applying a series of spikes of different amplitudes (-4, -6, -8, -10, -12 V). The duration of each spike was maintained constant, i.e., t_P = 90 s. Again, an external magnetic field of 10 kOe was applied throughout the measurements to magnetically saturate the generated ferromagnetic counterpart. As shown in **Figure 4**a, M increases with increasing spike amplitude (more negative), due to a more pronounced paramagnetic-to-ferromagnetic phase transformation at a higher voltage. The increment of M with electrolyte-gating occurs due to the combined contribution of the electrostatic effect and electrochemical reaction driven by the EDL. The latter involves denitriding of the sample assisted by the electric field. Furthermore, the increment/decrement in sample M with negative/positive gating is analogous to the excitatory/inhibitory behavior of the magnetic synapse. While Figure 4a presents the excitatory behavior at different spike amplitudes, the inhibitory behavior of the CoFeN based synapse is mimicked by applying spike (V_G = 10 V, t_P = 50 s), presented Figure S4 (in Supporting Information).

Figure 4a reveals that M increases during 90 s of spike application, however, after spike removal, M relaxes tending to level off after 1500 s. The relaxation in M represents volatile magnetic changes, that can be used to mimic the short-term plasticity in the human brain. Remarkably, M retains a constant and voltage-tunable value for a longer time, presenting the non-volatile magnetic change analogous to long-term plasticity. The resultant M_S is plotted as a function of spike amplitude in Figure 4b. The M_S measured immediately after spike removal (at peak) is defined as volatile change, while the M_S measured after 2000 s from spike

ADVANCED
SCIENCE NEWS

www.advancedsciencenews.com

ADVANCED
ELECTRONIC
MATERIALS
Open Access
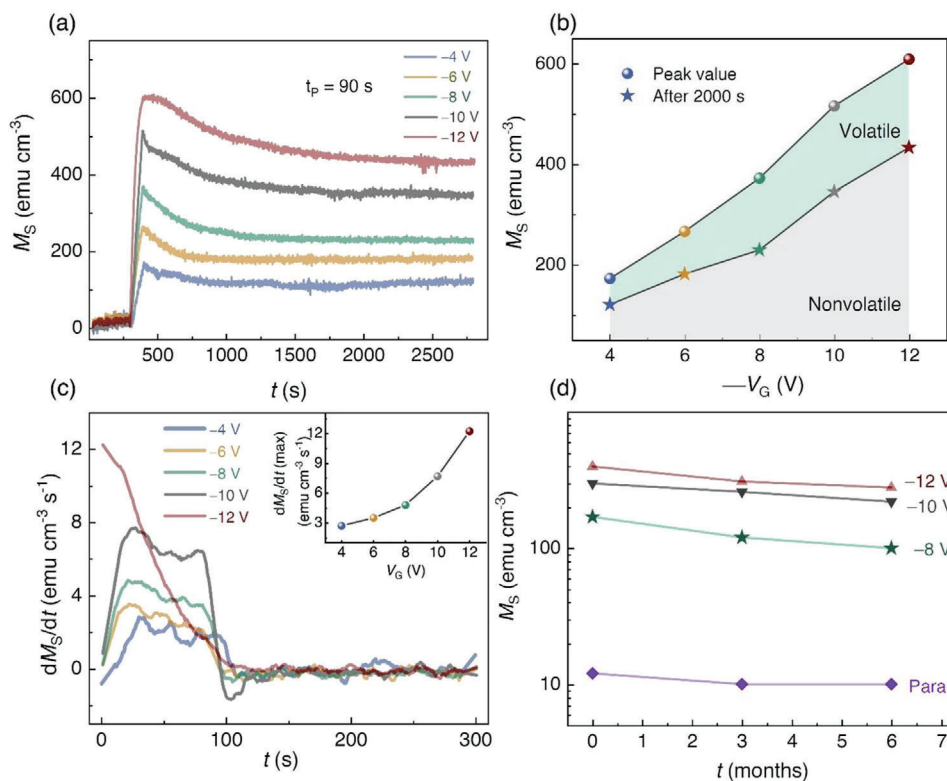
www.advelectronicmat.de

Figure 4. a) Spike amplitude-dependent plasticity emulated by firing spikes of different amplitudes (-4, -6, -8, -10, and -12 V) and of the same duration (t_P = 90 s). b) Change in M as a function of spike amplitude. ΔM values were measured immediately (at peak) and after 2000 s of spike removal, presenting volatile and non-volatile changes, respectively. c) Time derivative of magnetization for different spike amplitudes (the inset shows the maximum magneto-ionic speed as a function of spike amplitude). d) Retention of the device treated at different gate voltages. After electrolyte gating in liquid, the sample was stored at ambient, and the M was measured at air periodically. The initial state (non-treated sample) is denoted as "Para".

removal is defined as non-volatile change.[47] Both the volatile and non-volatile M_S contributions increase monotonically as a function of V_G, representing the complete emulation of SADP.

Device speed is an important figure of merit of a synaptic device. The speed of the magnetic switching determines the speed of the device. The rate of change of M (magneto-ionic speed) during the first 90 s of voltage application has been calculated by plotting the dM/dt for different spike amplitudes, as shown in Figure 4c. The speed of the device increases systematically as a function of spike amplitude, as presented in the inset. The investigated CoFeN-based synaptic device exhibits higher speed (12.3 emu cm^{-3} s^{-1}) at room temperature, even at a much lower voltage (-12 V) compared to other magneto-ionic systems, which is very promising for practical NC applications. For instance, 85 nm thick CoN and FeN exhibits magneto-ionic speed of 0.7 and 0.1 emu cm^{-3} s^{-1} respectively, with an applied voltage of -50 V.[34,48] Even thinner (5 nm) films of CoN and Co_3O_4 exhibits lower speed of 5.9 and 1.1 emu cm^{-3} s^{-1} with higher applied voltages of −25 and -50 V, respectively.[36,49] Furthermore, sample retention is crucial for the hardware implementation of NC. Figure 4d shows the retention of the voltage-treated samples at different amplitudes. For retention check, first the samples were voltage treated in the liquid electrolyte and immediately removed to ambient for M measurement. Later on, the samples were stored in the ambient and the M were measured periodically, showing the long-term stability and high retention of the voltage-treated sample in air.

The CoFeN-based synaptic device shows remarkable retention in ambient of at least six months (till we measure). M is particularly stable for the high voltage treated sample due to the dominant denitriding that causes a non-volatile change. Moreover, the energy consumption of the device is ≈120 µJ spike^{-1}. The larger energy consumption is attributed to the huge device size (≈several mm^2), which can be scaled down by lithography patterning (to nanoscale regime) to have energy consumption comparable to biological synapses.[9,50,15]

Similarly, extending the spike duration is another means to tune the synaptic connection, termed "spike duration-dependent plasticity" (SDDP). To mimic SDDP in the nitride-based synaptic device, spikes of different duration (30, 60, 90, 120, 150 s) and the same amplitude (-8 V) were fired to the gate terminal. A magnetic field of 10 kOe was applied to the sample throughout the measurement to saturate M. The results are shown in **Figure 5**a. With increasing the spike duration, the attained M value becomes progressively larger, strengthening the synaptic connection. In fact, during spike application, M_S increases, while after spike removal, there is a relaxation of M, again leading to volatile and non-volatile components of M_S, similar to the SADP experiments. The M_S variation with spike duration is summarized in Figure 5b. The M_S values measured immediately after spike removal represents the volatile change. In turn, the M_S measured after 2000 s of spike removal represents the non-volatile change. The volatile change is mainly attributed to electrostatic effects and it represents short-term plasticity. The redistribution of N ions inside the
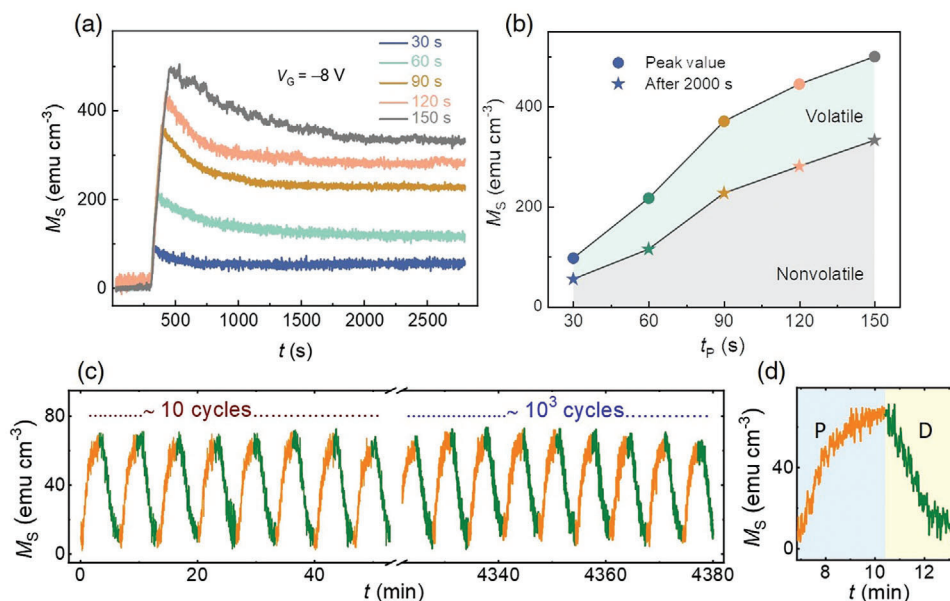
**ADVANCED
SCIENCE NEWS**

www.advancedsciencenews.com

**ADVANCED
ELECTRONIC
MATERIALS**

www.advelectronicmat.de

Figure 5. a) Spike duration-dependent plasticity mimicked by applying a series of spikes of different durations (30, 60, 90, 120, 150 s) and the same amplitude (V_G = -8 V). b) The variation of ΔM as a function of spike duration for both volatile and non-volatile change. c) Several cycles of potentiation and depression were realized in the nitride-based synaptic device, illustrating excellent endurance. d) The enlarged view of a single cycle of potentiation (P) / depression (D).

thin films after voltage treatment also contributes to the volatile change of sample M. The non-volatile change, caused by the denitriding process, represents long-term plasticity. Figure 5b shows that the M_S increases monotonically with spike duration due to more sample denitriding with longer spikes, causing a more pronounced paramagnetic to ferromagnetic phase transition.

Long-term plasticity is a very important form of synaptic plasticity, that constitutes the basis for learning and memory in the human brain.[51] By applying a series of consecutive pulses, we could emulate the long-term potentiation (LTP) and long-term depression (LTD) in the nitride-based synaptic device. LTP was mimicked by applying a series of ten negative pulses (V_G = -8 V, t_P = 10 s, spaced apart by Δt = 10 s). This results in a massive increment in M due to sample denitriding. M was then brought back to the initial state with a series of ten consecutive positive pulses (V_G = 8 V, t_P = 10 s, Δt = 10 s), emulating LTD. During LTD/LTP the sample undergoes denitriding/nitriding with successive pulses. Figure 5c shows several cycles of potentiation (P) and depression (D) mimicked in the synaptic device. The device could be cycled > 10^3 times without undergoing any degradation, exhibiting excellent cyclability and endurance for practical NC applications. Figure 5d shows an enlarged view of one cycle of potentiation and depression.

3. Conclusion

A magneto-ionic-based synaptic device based on CoFeN, where we have used voltage-induced magnetic switching to emulate biological synapses, is proposed. The strong (880 emu cm^{-3}) and fast (12.3 emu cm^{-3} s^{-1}) magneto-ionic response make the device promising for NC. The insertion/removal of N^{3-} ions, responsible for such magnetic switching, have been experimentally demonstrated. We have realized multilevel non-volatile mag-

netic states for analog computing and multi-state storage using programmed voltage pulses. Furthermore, representative synaptic functions such as spike amplitude-dependent plasticity, spike duration-dependent plasticity, and long-term potentiation/depression have been mimicked in the device. Interestingly, we have realized excellent endurance ($\approx 10^3$) and remarkable retention time (≈ 6 months), turning it into a suitable device for real-life implementation in NC. The study suggests that the proposed magneto-ionic-based synaptic device with multilevel storage may have great application prospects in spin-based NC.

4. Experimental Section

Sample Fabrication: The CoFeN thin films were deposited on Ti (20 nm)/Cu (60 nm) coated [100]-oriented Si substrate using AJA International ATC 2400 sputtering system with a base pressure of $\approx 10^{-8}$ Torr. High-purity Ar: N$_2$ (50%:50%) environment with a pressure of 3×10^{-3} Torr was maintained during the nitride film growth. The films were deposited at room temperature with a sputtering speed of 0.5 Å s^{-1}. One portion of the sample was masked during deposition to leave the Ti/Cu layer exposed to later make the contact and let it act as the working electrode.

Magnetoelectric Measurement: All the magnetoelectric measurements were carried out at room temperature, applying voltage in a capacitor-like configuration. A platinum wire was used as the counter electrode. An anhydrous propylene carbonate with dissolved Na$^+$ (10–25 ppm) was used as the gate electrolyte, where metallic sodium was used to eliminate any traces of residual water in the electrolyte. The in situ magnetic measurements were carried out using a VSM (Micro Sense LOT-Quantum design) with a maximum in-plane magnetic field of 20 kOe. The M-H loops were corrected for the linear slope at high fields to remove the diamagnetic/paramagnetic contributions from the Si substrate and the VSM holder. The voltage pulses were applied using an Agilent B2902A power supply to emulate neuromorphic functionalities.

Structural Characterization: XPS measurements were carried out using a PHI 5500 Multitechnique System (Physical Electronics), with a

monochromatic Al Kα (E = 1486.6 eV) source. The XPS measurements were carried out ex situ, immediately after voltage treatment of the samples, and subsequently washing them using deionized water. CasaXPS software was used for XPS peak deconvolution and a Shirley background was used for all elements.

Supporting Information

Supporting Information is available from the Wiley Online Library or from the author.

Conflict of Interest

The authors declare no conflict of interest.

Data Availability Statement

The data that support the findings of this study are available from the corresponding author upon reasonable request.

[1] J. Backus, *Commun. ACM* **1978**, *21*, 613.
[2] S.-T. Yang, X.-Y. Li, T.-L. Yu, J. Wang, H. Fang, F. Nie, B. He, L. Zhao, W.-M. Lü, S.-S. Yan, A. Nogaret, G. Liu, L.-M. Zheng, *Adv. Funct. Mater.* **2022**, *32*, 2202366.
[3] S. Boyn, J. Grollier, G. Lecerf, B. Xu, N. Locatelli, S. Fusil, S. Girod, C. Carrétéro, K. Garcia, S. Xavier, J. Tomas, L. Bellaiche, M. Bibes, A. Barthélémy, S. Saïghi, V. Garcia, *Nat. Commun.* **2017**, *8*, 14736.
[4] S. G. Sarwat, B. Kersting, T. Moraitis, V. P. Jonnalagadda, A. Sebastian, *Nat. Nanotechnol.* **2022**, *17*, 507.
[5] D. Kuzum, R. G. D. Jeyasingh, B. Lee, H.-S. P. Wong, *Nano Lett.* **2012**, *12*, 2179.
[6] S. Paramanik, A. Maiti, S. Chatterjee, A. J. Pal, *Adv. Electron. Mater.* **2022**, *8*, 2100237.
[7] F. Zhou, Z. Zhou, J. Chen, T. H. Choy, J. Wang, N. Zhang, Z. Lin, S. Yu, J. Kang, H. S. P. Wong, Y. Chai, *Nat. Nanotechnol.* **2019**, *14*, 776.
[8] Q. Wang, T. Zhao, C. Zhao, W. Liu, L. Yang, Y. Liu, D. Sheng, R. Xu, Y. Ge, X. Tu, H. Gao, C. Zhao, *Adv. Electron. Mater.* **2022**, *8*, 2101260.
[9] W. Xu, S. Y. Min, H. Hwang, T. W. Lee, *Sci. Adv.* **2016**, *2*, 1501326.
[10] C. Ge, C. xiang Liu, Q. li Zhou, Q. hua Zhang, J. yu Du, J. kun Li, C. Wang, L. Gu, G. zhen Yang, K. juan Jin, *Adv. Mater.* **2019**, *31*, 1900379.
[11] Q. Zhang, Y. Zhao, C. He, Y. Huo, B. Cui, Z. Zhu, G. Zhang, G. Yu, B. He, Y. Zhang, H. Lyu, Y. Guo, J. Qi, S. Shen, H. Wei, B. Shen, S. Wang, *Adv. Electron. Mater.* **2022**, *8*, 2200845.
[12] J. Liu, T. Xu, H. Feng, L. Zhao, J. Tang, L. Fang, W. Jiang, *Adv. Funct. Mater.* **2022**, *32*, 2107870.
[13] G. W. Burr, R. M. Shelby, A. Sebastian, S. Kim, S. Kim, S. Sidler, K. Virwani, M. Ishii, P. Narayanan, A. Fumarola, L. L. Sanches, I. Boybat, M. Le Gallo, K. Moon, J. Woo, H. Hwang, Y. Leblebici, *Adv Phys X* **2017**, *2*, 89.
[14] J. Grollier, D. Querlioz, K. Y. Camsari, S. Fukami, M. D. Stiles, *Nat. Electron.* **2020**, *3*, 360.
[15] D. Kumar, H. J. Chung, J. Chan, T. Jin, S. Ter Lim, S. S. P. Parkin, R. Sbiaa, S. N. Piramanayagam, *ACS Nano* **2023**, *17*, 6261.
[16] X. Zhang, W. Cai, M. Wang, B. Pan, K. Cao, M. Guo, T. Zhang, H. Cheng, S. Li, D. Zhu, L. Wang, F. Shi, J. Du, W. Zhao, *Adv. Sci.* **2021**, *8*, 2004645.
[17] R. Chen, C. Li, Y. Li, J. J. Miles, G. Indiveri, S. Furber, V. F. Pavlidis, C. Moutafis, *Phys. Rev. Appl.* **2020**, *14*, 014096.
[18] K. M. Song, J. S. Jeong, B. Pan, X. Zhang, J. Xia, S. Cha, T. E. Park, K. Kim, S. Finizio, J. Raabe, J. Chang, Y. Zhou, W. Zhao, W. Kang, H. Ju, S. Woo, *Nat. Electron.* **2020**, *3*, 148.
[19] Y. Huang, W. Kang, X. Zhang, Y. Zhou, W. Zhao, *Nanotechnology* **2017**, *28*, 08LT02.
[20] T. Leonard, S. Liu, M. Alamdar, H. Jin, C. Cui, O. G. Akinola, L. Xue, T. P. Xiao, J. S. Friedman, M. J. Marinella, C. H. Bennett, J. A. C. Incorvia, *Adv. Electron. Mater.* **2022**, *8*, 2200563.
[21] R. S. Yadav, P. Gupta, A. Holla, K. I. Ali Khan, P. K. Muduli, D. Bhowmik, *ACS Appl. Electron. Mater.* **2023**, *5*, 484.
[22] Y. Cao, A. W. Rushforth, Y. Sheng, H. Zheng, K. Wang, *Adv. Funct. Mater.* **2019**, *29*, 1808104.
[23] J. Zhou, J. Chen, *Adv. Electron. Mater.* **2021**, *7*, 2100465.
[24] V. Milo, G. Malavena, C. M. Compagnoni, D. Ielmini, *Materials* **2020**, *13*, 166.
[25] B. Sun, G. Zhou, L. Sun, H. Zhao, Y. Chen, F. Yang, Y. Zhao, Q. Song, *Nanoscale Horiz.* **2021**, *6*, 939.
[26] D. A. Gilbert, A. J. Grutter, E. Arenholz, K. Liu, B. J. Kirby, J. A. Borchers, B. B. Maranville, *Nat. Commun.* **2016**, *7*, 12264.
[27] A. Molinari, H. Hahn, R. Kruk, *Adv. Mater.* **2019**, *31*, 1806662.
[28] M. Ameziane, R. Mansell, V. Havu, P. Rinke, S. van Dijken, *Adv. Funct. Mater.* **2022**, *32*, 2113118.
[29] G. Wei, L. Wei, D. Wang, Y. Chen, Y. Tian, S. Yan, L. Mei, J. Jiao, *Appl. Phys. Lett.* **2017**, *110*, 062404.
[30] A. J. Tan, M. Huang, C. O. Avci, F. Büttner, M. Mann, W. Hu, C. Mazzoli, S. Wilkins, H. L. Tuller, G. S. D. Beach, *Nat. Mater.* **2019**, *18*, 35.
[31] G. Chen, C. Ophus, A. Quintana, H. Kwon, C. Won, H. Ding, Y. Wu, A. K. Schmid, K. Liu, *Nat. Commun.* **2022**, *13*, 1350.
[32] D. B. Strukov, R. S. Williams, *Appl. Phys. A* **2009**, *94*, 515.
[33] M. Huang, M. U. Hasan, K. Klyukin, D. Zhang, D. Lyu, P. Gargiani, M. Valvidares, S. Sheffels, A. Churikova, F. Büttner, J. Zehner, L. Caretta, K. Y. Lee, J. Chang, J. P. Wang, K. Leistner, B. Yildiz, G. S. D. Beach, *Nat. Nanotechnol.* **2021**, *16*, 981.
[34] J. de Rojas, A. Quintana, A. Lopeandía, J. Salguero, B. Muñiz, F. Ibrahim, M. Chshiev, A. Nicolenco, M. O. Liedke, M. Butterling, A. Wagner, V. Sireus, L. Abad, C. J. Jensen, K. Liu, J. Nogués, J. L. Costa-Krämer, E. Menéndez, J. Sort, *Nat. Commun.* **2020**, *11*, 5871.
[35] Z. Tan, S. Martins, M. Escobar, J. De Rojas, F. Ibrahim, M. Chshiev, A. Quintana, A. Lopeandia, L. Costa-kr, E. Men, J. Sort, *ACS Appl. Mater. Interfaces* **2022**, *14*, 44581.
[36] Z. Tan, J. de Rojas, S. Martins, A. Lopeandia, A. Quintana, M. Cialone, J. Herrero-Martín, J. Meersschaut, A. Vantomme, J. L. Costa-Krämer, J. Sort, E. Menéndez, *Mater. Horiz.* **2023**, *10*, 88.

[37] G. Scheunert, O. Heinonen, R. Hardeman, A. Lapicki, M. Gubbins, R. M. Bowman, *Appl. Phys. Rev.* **2016**, *3*, 011301.

[38] A. Ghemes, O. Dragos-Pinzaru, H. Chiriac, N. Lupu, M. Grigoras, D. Shore, B. Stadler, I. Tabakovic, *J. Electrochem. Soc.* **2016**, *164*, D13.

[39] Y. Van De Burgt, A. Melianas, S. T. Keene, G. Malliaras, A. Salleo, *Nat. Electron.* **2018**, *1*, 386.

[40] J. Li, Z. Li, F. Ning, L. Zhou, R. Zhang, M. Shao, M. Wei, *ACS Omega* **2018**, *3*, 1675.

[41] J. Yu, Y. Zhong, X. Wu, J. Sunarso, M. Ni, W. Zhou, Z. Shao, *Adv. Sci.* **2018**, *5*, 1800514.

[42] A. Rajan, M. Sharma, N. K. Sahu, *Sci. Rep.* **2020**, *10*, 15045.

[43] K. Idczak, R. Idczak, R. Konieczny, *Phys. B Condens. Matter* **2016**, *491*, 37.

[44] M. B. Kennedy, *Cold Spring Harb. Perspect. Biol.* **2013**, *8*, a016824.

[45] P. Monalisha, S. Li, T. Jin, P. S. A. Kumar, S. N. Piramanayagam, *Nanotechnology* **2023**, *34*, 165201.

[46] B. Zhang, W. Lv, Y. Guo, B. Wang, K. Luo, W. Li, J. Cao, *Adv. Electron. Mater.* **2022**, *9*, 2200939.

[47] P. Monalisha, S. Li, T. Jin, P. S. A. Kumar, S. N. Piramanayagam, *J. Phys. D Appl. Phys.* **2022**, *56*, 015302.

[48] J. De Rojas, J. Salguero, F. Ibrahim, M. Chshiev, A. Quintana, A. Lopeandia, M. O. Liedke, M. Butterling, E. Hirschmann, A. Wagner, L. Abad, J. L. Costa-Krämer, E. Menéndez, J. Sort, *ACS Appl. Mater. Interfaces* **2021**, *13*, 30826.

[49] S. Martins, J. De Rojas, Z. Tan, M. Cialone, A. Lopeandia, J. Herrero-Martin, J. L. Costa-Kramer, E. Menendez, J. Sort, *Nanoscale* **2022**, *14*, 842.

[50] Y. Lee, H. L. Park, Y. Kim, T. W. Lee, *Joule* **2021**, *5*, 794.

[51] D. V. Buonomano, W. Maass, *Nat. Rev. Neurosci.* **2009**, *10*, 113.